JOURNAL OF FOOD ENGINEERING (2020) 268:109745

https://doi.org/10.1016/j.jfoodeng.2019.109745

THERMOGRAPHIC STUDIES OF COCURRENT AND MIXED FLOW SPRAY DRYING OF HEAT SENSITIVE BIOACTIVE COMPOUNDS

Obón* J.M.[a], Luna-Abad J.P.[b], Bermejo B.[a], Fernández-López, J.A.[a]

(a) Departamento de Ingeniería Química y Ambiental. (b) Departamento de Ingeniería Térmica y de Fluidos. Universidad Politécnica de Cartagena. Spain

***Corresponding author e-mail:** josemaria.obon@upct.es (José María Obón)

Contact details: Departamento de Ingeniería Química y Ambiental
Universidad Politécnica de Cartagena
Paseo Alfonso XIII, 52, E-30203 Cartagena (Murcia), Spain
Phone: + 34 968 32 55 64 Fax: + 34 968 32 55 55

Authors e-mail: jp.lunabad@upct.es (Juan Pedro Luna-Abad)
bartolo.bh@gmail.com (Bartolomé Bermejo)
josea.fernandez@upct.es (José Antonio Fernández-López)

Submitted to: **Journal of Food Engineering**

Short title: Thermography of spray drying bioactive compounds

Keywords: cocurrent spray drying; mixed-flow spray drying; thermography; enzymes; natural colorants; microencapsulation

Abstract

Production of powders of heat sensitive bioactive compounds in a bench scale spray drier was studied under cocurrent and mixed flow pattern conditions using two inlet air temperatures of 200 and 120 ºC. Two natural colorants (riboflavin-5-phosphate and red beet) and an enzyme (alpha-amylase), were selected for experimentation. Thermographic studies showed interesting asymmetric profiles of temperatures outside and inside of the drying chamber, because turbulent air flow conditions and thermal trajectories of atomized drops during its drying process were dependent on flow patterns. Powders of natural colorants maintained its color strength, and alpha-amylase powders retain more than 82.9% of its enzyme activity even at the highest air temperature of 200 ºC and using mixed flow. This work concludes that spray drying under cocurrent and mixed-flow patterns of heat labile bioactive compounds is feasible, influencing drying yields and the properties of powders obtained.

1. Introduction

Spray drying is a well-known technique to formulate food powders (Murugesan & Orsat, 2012; Ray et al., 2016; Fang & Bhandari, 2017). It plays an important role in microencapsulation of natural ingredients as antioxidants, colorants, enzymes or cells used for the food industry. Microencapsulation protects bioactive compounds from light, temperature or oxygen during storage, and can affect its release behavior during digestion (Gharsallaoui et al., 2007; Barbosa & Teixeira, 2017; Guerin et al., 2017; Wang et al., 2018).

Spray drying process comprises three phases: the atomization of the liquid stream, the drying phase with the formation of solid product particles and the collection of powders. All these phases are important but the drying in the chamber has a huge effect on the drying process efficacy and the final product properties. In the chamber, liquid atomized droplets move through different trajectories due to the turbulent drying air gas flow inside, so each droplet loses its water content under different conditions of temperature and humidity. Contact patterns of atomized liquid droplets and drying air gas flow inside the drying chamber can be classified as cocurrent, countercurrent and mixed-flow. In mixed-flow pattern atomized droplets passes countercurrent and then cocurrent with drying air gas flow. Cocurrent spray dryers are the most widely used in comparison with countercurrent, and mixed-flow dryers are a good option to dry thermostable products (Cal & Sollohub, 2010; Keshani et al. 2015). Selection of contact pattern in drying chamber and spray drying conditions are critical to avoid damage or inactivation during the spray drying process of natural compounds such as vitamins, enzymes or cells that are thermolabile (Yoshii et al., 2008; Schutyser et al., 2012).

There is a high number of studies that optimize spray drying conditions using factorial experimental design in order to improve powder properties and to maximize product

yields (Singh & Singh-Hathan, 2017; Focaroli et al., 2019; Nair et al., 2019). In all cases a good knowledge of spray drying fluid dynamics would help researchers to select properly the operation conditions of the equipment.

The aim of this work was to evaluate the spray drying of thermolabile bioactive compounds under cocurrent and mixed flow conditions, working with a worldwide used bench-scale Mini Spray dryer. This study selected three commercial bioactive preparations: two water-soluble natural colorants and an enzyme. Riboflavin-5-phosphate or flavin mononucleotide (FMN) is the phosphorylated form of vitamin B_2 (riboflavin), an enzyme cofactor, and it is commercialized pure as an orange colorant powder (Choe et al., 2005; Sheraz et al., 2014). Red beet is a red-purple colorant extract and its color is due to betalains, a mix of red-purple betacyanins and yellow betaxanthins. This colorant is moderately stable, and it is commercialized as a microencapsulated powder obtained by spray drying from a blend of red beet juice and maltodextrin as drying aid (Fernández-López et al., 2013; Khan, 2016). Alpha-amylase (1,4-α-D-Glucan-glucanohydrolase; EC 3.2.1.1) from *Aspergillus oryzae* is an enzyme widely used in the food industry that breaks down soluble starch (Gupta et al., 2003). A special emphasis was paid to the effect of temperature; as different spray patterns offer diverse thermal degradation of bioactive compounds. The study measure for the first time to our knowledge simultaneous temperature profiles in the surface (thermographic images) and inside of the drying chamber (thermocouples) under cocurrent and mixed flow conditions.

2. Materials and methods

2.1. Materials

The natural colorants riboflavin-5-phosphate (E-101) and red beet powder (E-162) were kindly supplied by PROQUIMAC PFC, Barcelona, Spain. Crude α-amylase from

Aspergillus oryzae (30 U/mg) and dinitrosalycilic acid were purchased from SIGMA-ALDRICH, Madrid, Spain. Soluble starch, maltose 1-hydrate, and tartrate sodium-potassium were supplied by PANREAC QUÍMICA, S.A., Barcelona, Spain.

2.2. Spray drying equipment set-up

A bench-scale Mini Spray Dryer B-290 (Büchi Labortechnik AG, Flawil, Switzerland) was modified to be operated under cocurrent or mixed flow. An innovative glass cylinder (50 x 15 cm) was made with the same geometry that the original but bottom zone was adapted to locate a spray nozzle to spray the liquid upwards (Figure 1A). Working in cocurrent flow liquid was atomized with the upper spray nozzle and hot air travels downwards in the same direction, however, in mixed flow liquid was atomized with the bottom spray nozzle traveling upwards in the opposite direction of hot air first, and then in the same direction (Figure 1A). An atomization angle of 30º was calculated from photographs taken during water atomization and drawn in Figure 1A. Height of glass cylinder was graduated in centimetres from top (Figure 1A) and its circumference perimeter numbered from 1 to 8 (Figure 1B,1C) to facilitate drying chamber descriptions. Drying air enters from the top of the drying chamber through two symmetric semi-circular crowns, because in the middle is located the spray nozzle (Figure 1B). Drying air travelling through the semi-circular crown located in position 3 is divided in two because of the spray nozzle position, while air travelling through position 7 it is not divided. Inlet drying air travels faster through position 3. Outlet of drying air is located at 23º of plane 1-5 (Figure 1C). Temperatures on the surface of the glass cylinder were recorded during the spray drying process using a high resolution infrared FLIR T400 thermographic camera (Portland, Oregon, USA). Due to equipment configuration, thermographic images could only be taken from positions 1 to 5 (Figure 1C). Surface temperatures were followed in position 3 at four cylinder lengths H1-H4

(Figure 1A), and also in the cyclone upper zone. To measure the temperature inside the glass cylinder thermocouple tips were located at 0.5, 2, 4 and 6 cm from the centre, every 5 cm at ten different positions from the top (dots shown in Figure 1A and 1C). Four thermocouples were rotated together around central axis and moved vertically through drying chamber to measure all points. A total of 80 measurements were done in the plane of drying air flow exit (Figure 1C). A four channel temperature datalogger (4KDatalog, TC S.A., Madrid, Spain) acquired data from four stainless steel thermocouples of 1 mm diameter (Type K, class 1) done in the same set. Temperatures were measured as the average of three waves obtained in steady state, and data used to create filled contour plots with SigmaPlot for Windows v10.0 (Systat Software, Inc., USA).

2.3. Spray drying experiments

Liquid feeds were prepared dissolving powders of colorants or α-amylase in deionised water at 2% w/v. Inlet liquid was thermostated at 22 ºC, and feed at a fixed rate of 0.5 L/h (0.14 g/s) through a two-fluids atomizing nozzle working with a spray air flow-rate of 0.47 m^3/h. Atomization cone angle was 30º (Figure 1A). Drying air flow-rate was fixed to 18 m^3/h (80% of scale). Two inlet air temperatures were studied 120 and 200 ºC. Spray drying equipment was in a room thermostated at 25 ºC. Inlet air was from outside of the building and outlet air was also conducted outside of the building. Powders were collected with a high-performance cyclone in a collection vessel. Powders were placed in closed flasks, weighted, and characterized as soon as possible. Meantime, samples were stored in a fridge (4 ºC).

Drying process efficacy was evaluated by drying yield, retention of color strength or enzyme activity. Powders were weighted with an electronic balance Sartorius AX224 (Sartorius, Madrid, Spain), and drying yield of spray drying experiments calculated as:

$$\textit{Drying yield (\%)} = \frac{grams\ of\ powder\ obtained}{grams\ of\ initial\ solid\ of\ feed}\ \textit{x 100}$$

Thermostability of colorants during spray drying experiments was evaluated as color strength retention:

$$\textit{Color strength retention (\%)} = \frac{final\ color\ strength}{initial\ color\ strength}\ \textit{x 100}$$

Thermostability of α-amylase in spray drying experiments was evaluated as enzyme activity retention:

$$\textit{Enzyme activity retention (\%)} = \frac{final\ \ \alpha - amylase\ activity}{initial\ \alpha - amylase\ activity}\ \textit{x 100}$$

All different spray drying experimental conditions were done by triplicate.

2.4. Characterization of bioactive compound powders

Measurement of color strength. Colorant powders were prepared 0.005% w/v (riboflavin-5-phospahte) and 0.4% w/v (red beet) with deionised water, and its absorbance measured at 420 nm (riboflavin-5-phosphate) or 535 nm (red beet), versus a blank cell filled with distilled water, and within the linear range of the spectrophotometer (Agilent 8453, Waldbronn, Germany). Solids weight was considered in wet basis. Color strength was calculated as the absorbance of a 1% w/v dissolution measured at the maximum wavelength of the colorant.

Measurements of α-amylase activity. One unit (U) of α-amylase activity was defined as the amount of enzyme that liberates 1 μmol of maltose per minute at pH 6.0 and 25 ºC. Assay was adapted from Keharom et al. 2016, as follow: a reaction mixture of 4 ml starch solution (1% w/v) and 1 ml of enzyme solution were incubated at 25 ºC. Samples of 0.5 ml were withdrawn every 30 seconds for 5 min and mixed in test tubes with 0.5 ml of DNS reagent (Miller, 1959). Samples were incubated at 85 ºC for 10 min, diluted with 2 ml of water, and absorbance measured spectrophotometrically at 540 nm versus

158 a blank cell filled with a sample incubated with water and DNS. Maltose was the
159 standard of the calibration curve. Activity was calculated as:

160 Activity (µmol/min) = ΔAbsorbance/min x 5 (ml) / Calibration curve slope (Abs/mM)

161 *Measurements of water content*. Determinations were done following reduction in
162 weight of 5 g of the samples dried at 90 ºC in an oven (Digitheat, Selecta, Spain), until
163 obtaining a constant value. Weights were measured with an electronic balance
164 Sartorius AX224 of 0.1 mg precision (Sartorius, Madrid, Spain). Results were
165 calculated in wet basis and expressed as percentage in mass.

166 *Measurements of bulk density.* Bulk density was determined as tapped density by
167 weighting 3 g of a sample into a 10 ml graduated cylinder. Cylinder was vibrated
168 approximately 1500 taps to obtain a near optimum packing (Autotap, Quantachrome,
169 USA) (Miravet et al., 2016). When a steady volume was reached, volume was
170 measured, and density calculated as Kg/m^3.

171 *Dissolution test.* Dissolution test consisted in dissolving 2.50 g of powder in 50 ml of
172 water (solution 5%) by magnetic agitation (Agimatic S, Selecta, Spain) until obtaining a
173 clear solution (Miravet et al., 2016). Magnetic stirring was established at 1000 rpm, with
174 a 20 mm cylindrical stir bar and a 100 mL Erlenmeyer flask. The time to fully
175 reconstitute the powders and obtain a visually clear solution was measured in seconds.

176 *Particle morphology analysis*. A Scanning Electronic Microscopic HITACHI High
177 Technologies (S-3500N, Tokyo, Japan) was used to evaluate morphology and particle
178 size of spray-dried powders. Samples were fixed in adhesive tape placed into SEM
179 stubs before visualization. The sample surface was covered during 120 seconds by a
180 thin gold layer, being conductive. SEM worked with a voltage of 5 kV. Lens was placed
181 at 8 mm from the sample. Images were obtained from representative zones of samples
182 at a 5000 magnification.

183 *Statistical analysis*. All spray-drying experiments and analytical measurements were
184 done by triplicate. The mean values, standard deviations, and analysis of variance
185 (ANOVA) were calculated with Minitab statistic software, version 13.2 (Minitab Inc.,
186 State College, PA, USA). Mean comparisons were performed using Tukey's test ($p \leq 0.05$).
187
188
189 **3. Results and discussion**
190 *3.1. Temperature profiles of spray dryer operation with only drying air (no atomization)*
191 Initial studies to evaluate temperature profiles outside and inside of spray dryer were
192 run with no atomization using inlet air at 200 or 120 ºC. A thermographic camera
193 located perpendicular to position 3 of the drying chamber (Figure 1C) measured
194 surface temperatures from the beginning of inlet air heating until reaching steady state
195 conditions. Figure 2ABC shows thermographic images of surface temperatures after 5,
196 15 or 30 minutes of operation, using drying air at 200 ºC. In Figure 2C drying chamber
197 at steady state showed a first upper cold zone from top to about 6 cm height. It is cold
198 because hot air flow enters only thought the central part of the cylinder. Then a hot
199 second zone is observed due to the impact of hot air flow into the wall, and finally there
200 is a third zone with a descendent gradient of temperature as air flow travels to the exit.
201 The highest surface temperatures in the equipment were always measured in the
202 cyclone surface and the lowest in the collection vessel. Zoom images of the top of
203 drying chamber taken with the camera perpendicular to different positions from 1 to 4,
204 showed that temperatures in this zone were different at the same height (Figure 2DEF).
205 There were two hot dots in positions 2 and 3, which means that two inlet air flows hit at
206 similar rates at a cylinder height of 10 cm (H1). Positions 4 and 5 were cooler, and
207 position 1 was the coolest. It can be explained by the geometry of top air inlet (Figure

1B). These findings suggest that three main air jets process about the central axis and two of them are directed to the left part of the cylinder, opposite to air exit (positions 2-3). Turbulent flow is responsible of the location of the different recirculation zones between the main jets and the chamber wall observed in the thermographic images.

Figure 2G shows the evolution of surface temperatures on drying chamber at positions H1-H4 and cyclone. Steady-state temperatures were achieved after 25 minutes. Time to reach steady state temperatures were similar at the different heights of the drying chamber, however cyclone stabilize its surface temperatures sooner due to its higher air flow rates. The small radii of the cyclone chamber and exit duct cause a greater resistance to air flow through the cyclone and hence a greater pressure drop across it (Maury et al., 2005).

Experiments done using an air inlet temperature of 120 ºC showed similar images of surface temperatures, and upper hot dots in the same positions. Steady state conditions were achieved a bit later, after 30 minutes. The gradient of final surface temperatures from positions H1 to H4 was lower (11.6 ºC, from 65.8 to 54.2 ºC) than obtained previously with air at 200 ºC (22.4 ºC, from 95.7 to 73.3 ºC). An increase of air inlet temperature of 80 ºC resulted in a 20-30 ºC increase on surface temperatures. Heat loss can explain that the wall temperatures of drying chamber were not as high as could be expected when using the inlet drying air temperature of 200 ºC.

Measurements of air temperatures inside drying chamber are closely related with the surface temperatures of drying chamber previously explained. They can offer interesting information about expected air flow pattern and its effect on bioactive compounds thermoinactivation. Figure 3 shows a filled contour plot of temperatures measured with thermocouples located inside the drying chamber in the plane of air outlet. Equipment run with inlet air at 200 ºC, and temperatures were measured once

steady state was reached. The highest temperature values were obtained in the upper central part close to the inlet of hot air. It had only a 10 cm length, due to the turbulent flow inside the chamber. This is an important hot zone for drying. Contour plot also revealed that temperatures were not symmetric with central axis at the same height of cylinder, being lower in the half cylinder zone of air outlet and confirmed the turbulent air pattern inside the drying chamber. Presence of different zones of temperatures close to wall were quite coincident with the temperature map obtained in previous thermographic study. Figure 4 shows the evolution of temperatures measured in the half cylinder zone of air exit, working with inlet air at 200 ºC and 120 ºC. In both cases, temperatures located at inner positions of cylinder (0.5, 2 cm) decrease when air descend to its exit. This is the position of the hot inlet air jets. However, in the middle and outer positions (4, 6 cm) temperatures raise up to 15-20 cm (hot zone), and then stabilized up to 39 cm. Temperature profiles agrees with the expected complex dynamic of turbulent air flow inside the drying chamber. The values of temperature at 44 cm close to air exit were around 151 and 90 ºC using air at 200 and 120 ºC, respectively. These are like air outlet temperatures of 152 and 91 ºC measured with the outlet thermopar of the spray drier working with air at 200 and 120 ºC, respectively.

Air flow patterns and presence of significant air flow instabilities has been explained with turbulence models using computational fluid dynamics (CFD) (Kuriakose & Anandharamakrishnan, 2010). Initial CFD studies with a Büchi B-290 bench-scale spray dryer reported that the k-epsilon turbulence model was the most suitable to predict flow behavior in the dryer (Pin et al., 2014). A more complete work of Pinto et al., 2014 showed CFD simulations of air flow patterns in a Büchi B-290 spray dryer with recirculation zones fluctuating in size between the main central jet and the chamber walls. These authors described central asymmetry, so that half cylinder located close to

air exit had a different pattern that its opposite half cylinder. While half cylinder close to air exit had a main recirculation zone up to H3, and a second until H4, its opposite half had a first zone located approximately up to a 4 cm height, a second between H1-H2, a third between H2-H3, a forth between H3-H4, and a fifth from H4 until the end. Temperatures profiles and thermographic studies obtained in this work during drying chamber operation at steady state agrees well with CFD simulations results of Pinto et al., 2014.

3.2. Temperature profiles of spray dryer operation with water in cocurrent and mixed flow

Atomizing cone angles were measured changing the values of atomizing air and water flow rates. Cone angle depends mainly on atomizing air flow rate, it changes from 80º at 0.25 m^3/h (2 cm), to 50º at 0.36 m^3/h (3 cm), 30º at 0.47 m^3/h (4 cm), and 28º at 0.60 m^3/h (5 cm). Measurements in cm are related with the height of the rotameter scale used in the equipment. So, its suggested to use flow rates in the interval 0.47-0.6 m^3/h, because atomization with cone angles higher than 30 ºC would hit the wall of drying chamber (Figure 1). No remarkable effect of drying air flow rate on cone angle was observed.

In the following experiments, water was sprayed under cocurrent or mixed flow conditions using constant values of 0.47 m^3/h of air flow rate and 0.5 L/h of water flow rate. Equipment working with inlet air temperatures of 200 or 120 ºC reached steady state conditions after 20 minutes, then thermographic images were taken locating the camera perpendicular to position 3 of the drying chamber (Figure 5). In both cases is observed a descending gradient of temperature in the direction of air exit. Temperature gradients from H1 to H4 were smaller with cocurrent flow in comparison with mixed

283 flow. In mixed flow water enters from the bottom upwards and temperatures reached at
284 top positions are slightly higher. The lowest gradient H1-H4 was 2.7 ºC with cocurrent
285 flow, and the highest 13 ºC with mixed flow, both at 200 ºC. Temperatures in lower
286 zones are lower with mixed flow, thus cyclone surface temperatures are about 2.2 ºC
287 lower than those of cocurrent flow.

288 Temperature profiles were measured inside drying chamber in the half cylinder zone
289 of air outlet. Figure 6 shows temperatures at steady state conditions obtained during
290 spray drying of water under cocurrent or mixed flow conditions using inlet air
291 temperatures of 200 or 120 ºC. Water condensate in thermocouples located close to
292 nozzle tip so these temperature values were not included in graphs. Working with
293 cocurrent flow and 200 ºC, temperatures measured inside the drying chamber ranged
294 between 92 and 95 ºC. These results are in good agreement with temperatures of glass
295 surface where temperature gradient H1-H4 was only 2.7 ºC. At 120 ºC temperature of
296 outer thermocouples were higher than central ones, and temperature range inside
297 drying chamber was wider, in accordance with temperatures measured of glass
298 surface. In case of mixed flow and using an inlet air at 200 ºC, temperatures of
299 thermocouples were higher in the central core in the top zone of the cylinder. However,
300 from 14 cm onwards temperatures were lower in the center due to presence of sprayed
301 water drops. A similar pattern was observed using inlet air at 120 ºC. Temperature
302 gradients H1-H4 were between 62 and 98 ºC and are in good agreement with
303 temperatures of glass surface where it was found the widest temperature difference
304 between H1-H4. With mixed flow and air at 120 ºC temperatures inside drying chamber
305 were lower than 40 ºC between H1-H4, and the lowest of the different conditions
306 studied. These values also agree with the lowest surface temperatures measured with
307 mixed flow and 120 ºC.

Thermal studies show how air flow patterns inside drying chamber determine temperature profiles, and spray drying of bioactive compounds are expected to proceed at slightly higher temperatures with cocurrent flow versus mixed flow.

3.3. Spray drying of bioactive compounds under cocurrent and mixed flow patterns

Table 1 presents the results obtained of spray drying of bioactive compounds using cocurrent and mixed flow with inlet drying air at 200 and 120 ºC. The drying yields were always significantly higher at 200 ºC in comparison with 120 ºC. In addition, spray drying at 200 ºC led to particles of significant lower enzyme activity, higher bulk densities, lower water contents, and lower dissolution rates. These effects of temperature were independent of bioactive compound or flow pattern used. This dependence of temperature with drying yield is related to particle drying trajectories. If drying proceed insufficiently before impact with the wall, the particles can adhere, and hence drying yield is reduced. In case of spray drying trehalose (Maury et al., 2005) or soymilk (Nguyen et al., 2018) under cocurrent flow, higher drying yields and lower water contents were obtained increasing inlet temperatures.

Comparing the effect of pattern flow, cocurrent flow conditions presented with all bioactive compounds studied significant higher drying yields versus mixed flow, especially at 120 ºC. The highest drying yield of 75.5% was achieved with riboflavin-5-phosphate with cocurrent flow and 200 ºC, and the lowest 32% with the enzyme α-amylase with mixed flow and 120 ºC. Operation conditions using mixed flow at 120 ºC were not adequate for spray drying because of the low drying yields obtained. During spray drying of the two colorants no color loss was observed, and color yields were close to 100% under all spray drying conditions. Published studies also showed no significant changes in color parameters of beetroot powders with maltodextrin working

under cocurrent flow at 160 ºC using lab-scale or semi-industrial spray dryers (Koul et al., 2002; Janiszewska, 2014). In this work beetroot betalains were stable even under operation with mixed flow and air at 200 ºC. However, α-amylase enzyme activity was significantly affected by spray drying conditions. The best activity retention of 99.2% was achieved under cocurrent flow conditions using the inlet air temperature of 120 ºC, while lowest activity retention was 82.9% using mixed flow and 200 ºC. Operation at 200 ºC favor enzyme deactivation. Other authors spray dried α-amylase with lab scale equipments using cocurrent flow, and found a preservation of 83% of the initial activity at 145 ºC (de Jesus & Filho, 2014), and a range from 91.8 to 51.9% using air temperatures from 160 to 220 ºC (Samborska & Witrowa-Rajchert, 2005). In our experimentation, spray drying was an adequate technique to obtain powders of bioactive compounds as far as residence times of drying particles were short enough to minimize the denaturing effect of high temperatures, even with mixed flow.

Effect of flow pattern on particle properties as bulk density, water content or solubility were mainly dependent on bioactive compound properties. Powders of a pure compound as riboflavin-5-phosphate have significant higher bulk densities, lower water content and lower dissolution rates, under mixed flow operation at a similar temperature. However, flow pattern has no significant effect on densities, water content and dissolution rates of red beet and α-amylase powders. As an exception under mixed flow, red beet powder also shown lower water content and lower dissolution rates using drying air at 200 ºC, and α-amylase powders a higher bulk density at 120 ºC. The higher the bulk density, the lower the solubility of a powder is referenced by Fazaeli et al., 2012 for black mulberry powders.

Figure 7 compares the effect of flow pattern on the morphology of bioactive compounds obtained at 200 ºC. All particles have a spherical shape with diameters

ranged between 1-7 μm. No general differences in size or morphology for riboflavin 5 phosphate and red beet could be attributed to flow pattern used. Riboflavine 5 phosphate particles are small hollow spheres that have collapsed. Red beet powders had smooth surfaces and higher particle sizes, probably due to stickiness problems caused by sugars with low glass transition temperatures that are present in this vegetal juice. This morphology is well described in bibliography (Fazaeli et al., 2012; Miravet et al., 2016). Particles of α-amylase prepared by cocurrent flow are wrinkled, while prepared by the mixed flow appeared to be collapsed. The shape and size of particles are related to drying time and evaporation rate (Alamilla-Beltran et al., 2005), so it is feasible that particle trajectories during mixed flow facilitate water evaporation, resulting collapsed particles of lower water content.

Conclusions

Thermographic studies of the mini spray dryer working with hot air and without atomization showed asymmetric profiles of temperatures outside and inside of the drying chamber at steady state and corroborated the expected turbulent air flow conditions. There was a fast central core and different air recirculation zones inside the drying chamber related to the geometric position of inlet air flow and the direction of air exit. When water was spray dried in the equipment under cocurrent or mixed flow conditions thermal studies showed a predictable sharp decrease of temperature in the drying chamber, and slightly lower values were found with mixed flow. Water solutions of three heat labile bioactive compounds were spray dried using both flow patterns, and while colorant powders of riboflavin-5-phosphate and betalains maintained 100% its color, α-amylase retain more than 82.9% of its enzyme activity. It means that even when running with a high air temperature of 200 ºC it was feasible to produce powders

of heat labile compounds. Operation with cocurrent flow achieved higher drying yields versus mixed flow. Properties of bioactive powders were influenced by flow pattern. Bulk density was higher and water content lower with mixed flow. Results of this work encourage potential users to obtain novel food powders maintaining its bioactive compounds by spray drying.

Funding

This research did not receive any specific grant from funding agencies in the public, commercial, or not-for-profit sectors.

References

Alamilla-Beltrán, L., Chanona-Pérez, J.J:, Jiménez-Aparicio, A.R., & Gutiérrez-López, G.F. (2005). Description of morphological changes of particles along spray drying. *Journal of Food Engineering*, 67, 179–184.

Barbosa, J., & Teixeira, P. (2017). Development of probiotic fruit juice powders by spray-drying: A review. *Food Reviews International*, 33, 1525-6103.

Cal, K., & Sollohub, K. (2010). Spray Drying Technique. I: Hardware and Process Parameters. *Journal of Pharmaceutical Sciences*, 99, 575–586.

Choe, E., Huanf, R., & Min, D.B. (2005). Chemical reactions and stability of riboflavin in foods. *Journal of Food Science*, 70, 28–36.

de Jesus, S.S., & Filho R.M. (2014). Drying of α-amylase by spray drying and freeze-drying – a comparative study. *Brazilian Journal of Chemical Engineering*, 31(3), 625 - 631.

406 Fang, Z., & Bhandari, B. (2017). Spray Drying of Bioactives. In Y.H. Roos, Y.D. Livney
407 (Eds.), *Engineering Foods for Bioactives Stability and Delivery* (pp. 261-284). Springer,
408 New York.

409 Fernández-López, J.A., Angosto, J.M., Giménez, P.J., & León, G. (2013). Thermal
410 Stability of Selected Natural Red Extracts Used as Food Colorants. *Plant Foods for*
411 *Human Nutrition*, 68,11–17.

412 Fazaeli, M., Emam-Djomeh, Z., Ashtari, A.K., & Omid, M. (2012) Effect of spray drying
413 conditions and feed composition on physical properties of black mulberry juice
414 powder. *Food and Bioproducts Processing*, 90, 667-675.

415 Focaroli, S., Mah, P.T., Hastedt, J.E., Gitlin, I., Oscarson, S., Fahy, J.V., & Healy, A.M.
416 (2019). A Design of Experiment (DoE) approach to optimise spray drying process
417 conditions for the production of trehalose/leucine formulations with application in
418 pulmonary delivery. *International Journal of Pharmaceutics*, 562, 228-240.

419 Gharsallaoui, A., Roudaut, G., Chambin, O., Voilley, A., & Saurel, R. (2007).
420 Applications of spray-drying in microencapsulation of food ingredients: An overview.
421 *Food Research International*, 40, 1107–1121.

422 Guerin, J., Petit, J., Burgain, J., Borges, F., Bhandari, B., Perroud, C., Desobry, S.,
423 Scher, J., & Gaiani, C. (2017). *Lactobacillus rhamnosus* GG encapsulation by spray-
424 drying: Milk proteins clotting control to produce innovative matrices. *Journal of Food*
425 *Engineering*, 193, 10–19.

426 Gupta, R., Gigras, P., Mohapatra, H., Goswami, V.K., & Chauhan, B. (2003). Microbial
427 α-amylases: a biotechnological perspective. *Process Biochemistry*, 38, 1599-1616.

428 Janiszewska, E. (2014). Microencapsulated beetroot juice as a potential source of
429 betalain. *Powder Technology*, 264, 190-196.

Keharom, S., Mahachai, R., & Chanthai, S. (2016). The optimization study of α-amylase activity based on central composite design-response methodology by dinitrosalicylic acid method. *International Food Research Journal*, 23, 10-17.

Keshani, S., Daud, W.R.W., Nourouzi, M.M., Namvar, F., & Ghasemi, M. (2015). Spray drying: An overview on wall deposition, process and modeling. *Journal of Food Engineering*, 146, 152–162.

Khan, M.I. (2016). Stabilizations of betalains: A review. *Food Chemistry*, 197, 1280-1285.

Koul, V.K., Jain, M.P., Koul, S., Sharma, V.K., Tikoo, C.L., & Jain, S.M. (2002). Spray drying of beet root juice using different carriers. *Indian Journal of Chemical Technology*, 9, 442-445.

Kuriakose, R., & Anandharamakrishnan, C. (2010). Computational fluid dynamics (CFD) applications in spray drying of food products. *Trends in Food Science & Technology*, 21, 383-398.

Maury, M., Murphy, K., Kumar, S., Shi, L. & Lee, G. (2005) Effect of process variables on the powder yield of spray-dried trehalose on a laboratory spray-dryer. European *Journal of Pharmaceutics and Biopharmaceutics*, 59, 565-573.

Miller, G.L. (1959). Use of dinitrosalycilic acid reagent for determination of reducing sugar. *Analytical Chemistry*, 31, 426-428.

Miravet, G., Alacid, M., Obón, J.M., & Fernández-López, J.A. (2016) Spray-drying of pomegranate juice with prebiotic dietary fibre. *International Journal of Food Science and Technology*, 51, 633-640.

Murugesan, R., & Orsat, V. (2012). Spray Drying for the Production of Nutraceutical Ingredients—A Review. *Food and Bioprocess Technology*, 5, 3–14.

454 Nair, A., Khunt, D., & Misra, M. (2019). Application of quality by design for optimization
455 of spray drying process used in drying of Risperidone nanosuspension. *Powder*
456 *Technology*, 342, 156-165.
457 Nguyen, D.Q., Nguyen, T.H., Mounir, T.S. & Allaf, K. (2018) Effect of feed
458 concentration and inlet air temperature on the properties of soymilk powder obtained
459 by spray drying, *Drying Technology*, 36, 817-829.
460 Pin, C.S., Rashmi, W., Khalid, M., Chong, C.H., Woo, M.W., & Tee, L.H. (2014).
461 Simulation of spray drying on *Piper betle* Linn extracts using computational fluid
462 dynamics. *International Food Research Journal*, 21, 1089-1096.
463 Pinto, M., Kemp, I., Bermingham, S., Hartwig, T., & Bisten, A. (2014). Development of
464 an axisymmetric population balance model for spray drying and validation against
465 experimental data and CFD simulations. *Chemical Engineering Research and*
466 *Design*, 9(2), 619–634.
467 Ray, S., Raychaudhuri, U., & Chakraborty, R. (2016). An overview of encapsulation of
468 active compounds used in food products by drying technology. *Food Bioscience*,13,
469 76–83.
470 Samborska, K., & Witrowa-Rajchert, D. (2005). Spray-drying of α-amylase-The Effect
471 of Process Variables on the Enzyme Inactivation. *Drying Technology*, 23, 941–953.
472 Schutyser, M.A.I., Perdana, J., & Boom, R.M. (2012). Single droplet drying for optimal
473 spray drying of enzymes and probiotics. *Trends in Food Science & Technology*, 27,
474 73-82.
475 Sheraz, A.M., Kazi, S.H., Ahmed, S., Anwar, Z., & Ahmad, I. (2014). Photo, thermal
476 and chemical degradation of riboflavin. *Belstein Journal of Organic Chemistry*, 10,
477 1999-2012.

478 Singh, B., & Singh-Hathan, B. (2017). Process optimization of spray drying of beetroot
479 Juice. *Journal Food Science and Technology*, 54(8), 2241–2250.

480 Wang, S., Shi, Y., & Han, L. (2018). Development and evaluation of microencapsulated
481 peony seed oil prepared by spray drying: oxidative stability and its release behavior
482 during in-vitro digestion. *Journal of Food Engineering*, 231, 1-9.

483 Yoshii, H., Buche, F., Takeuchi, N., Terrol, C., Ohgawara, M., & Furuta, T. (2008).
484 Effects of protein on retention of ADH enzyme activity encapsulated in trehalose
485 matrices by spray drying. *Journal of Food Engineering*, 87, 34–39.

486

Figure 1

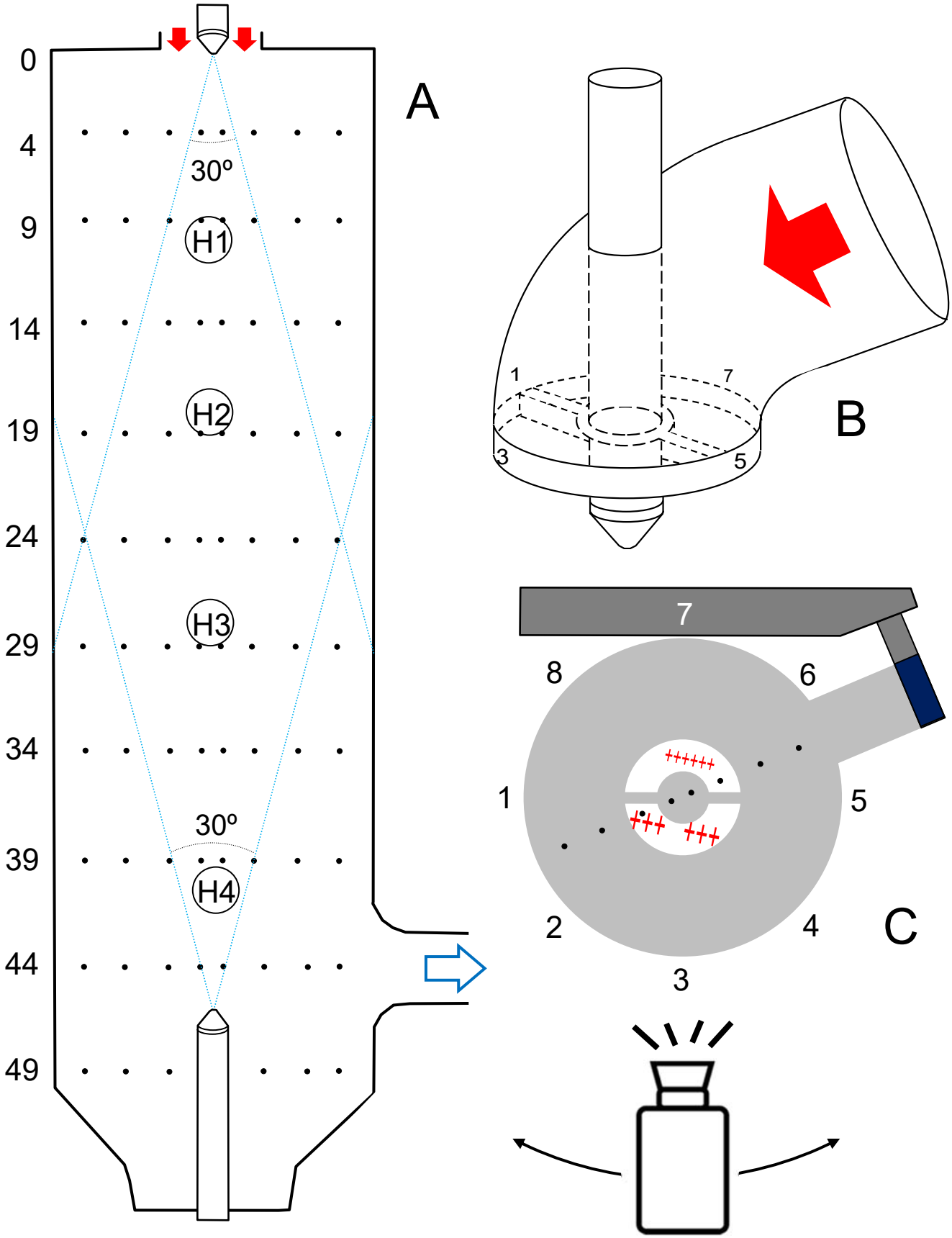

Figure 1

New Figure 2

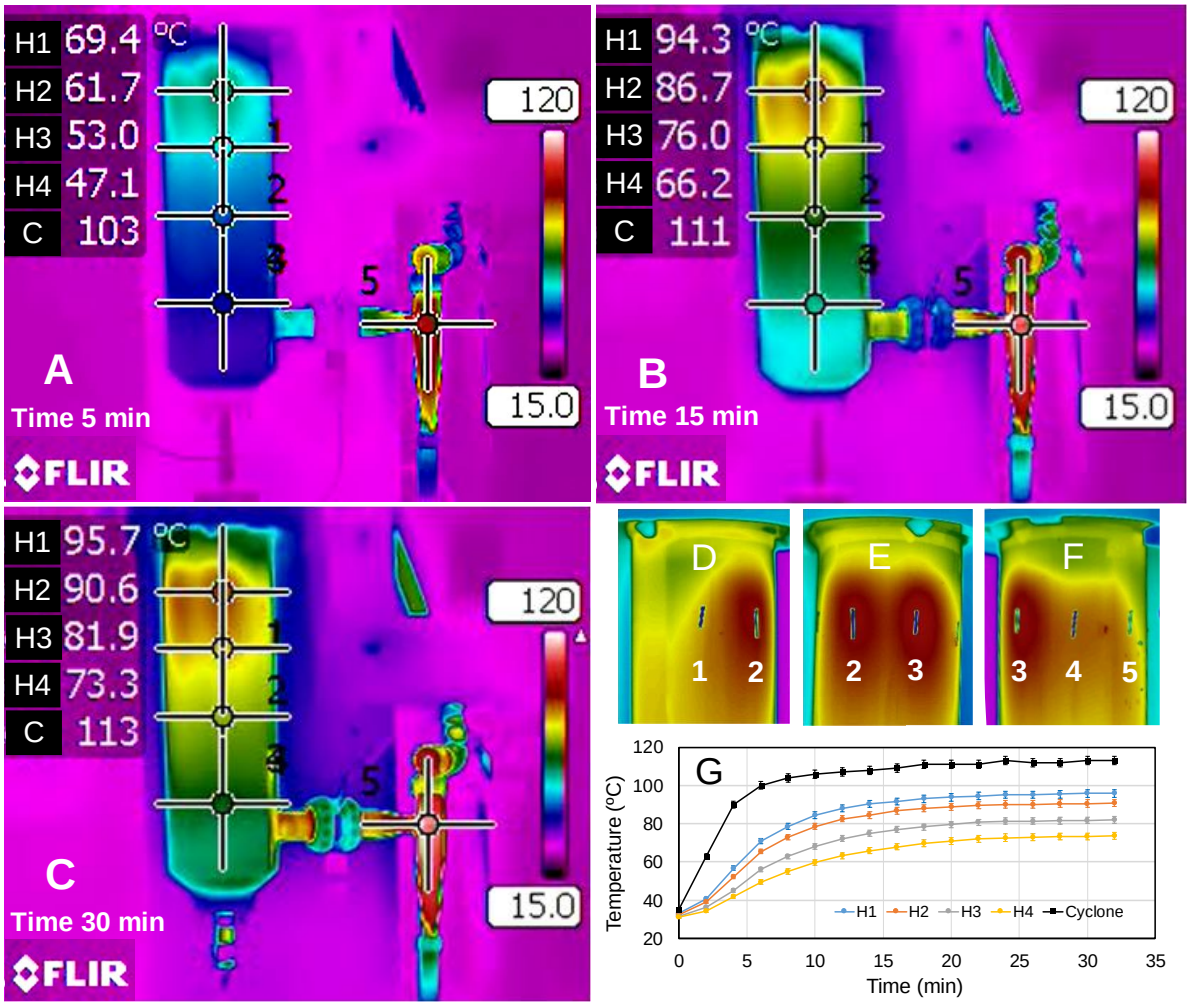

Figure 2

Figure 3

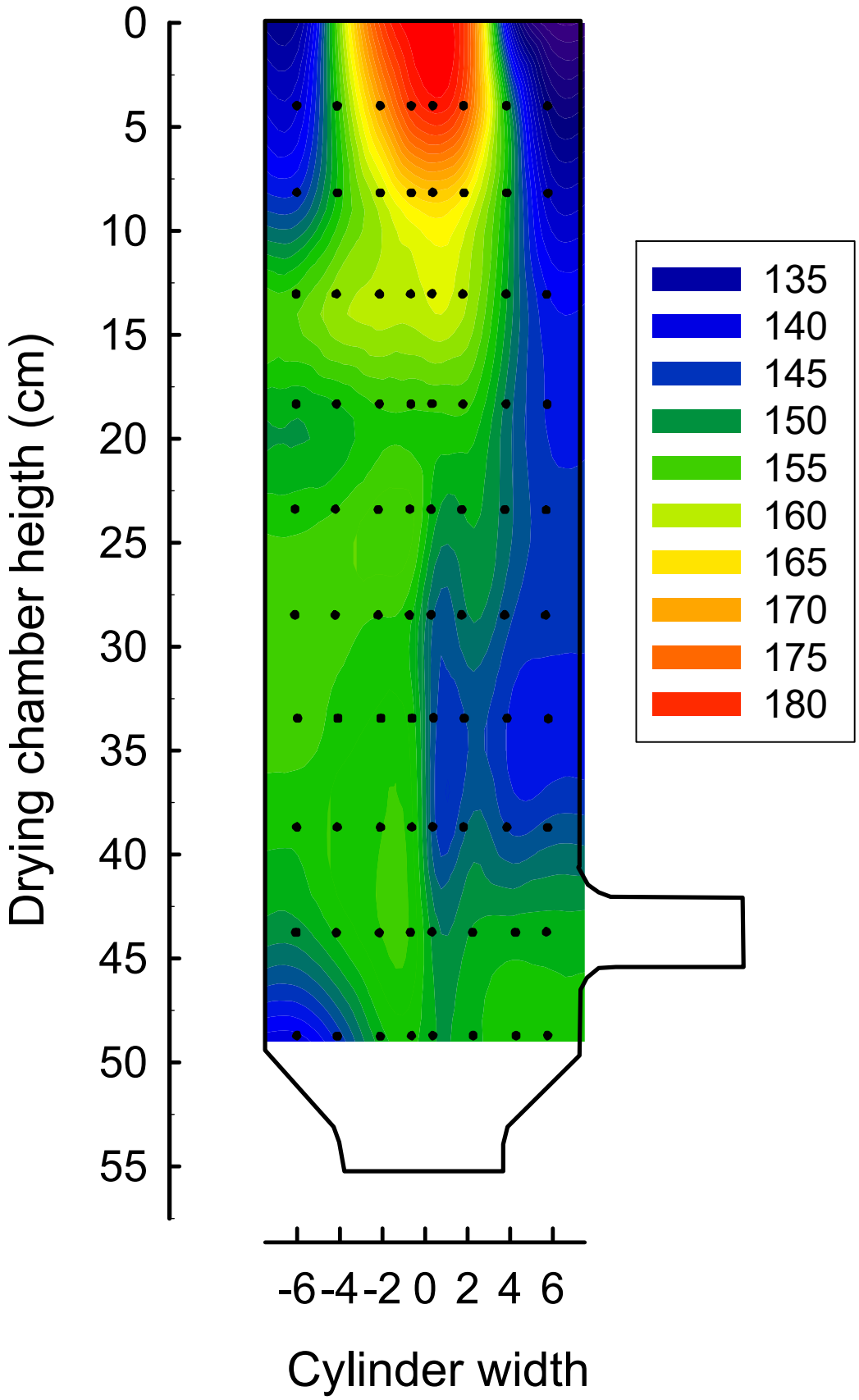

Figure 3

New Figure 4

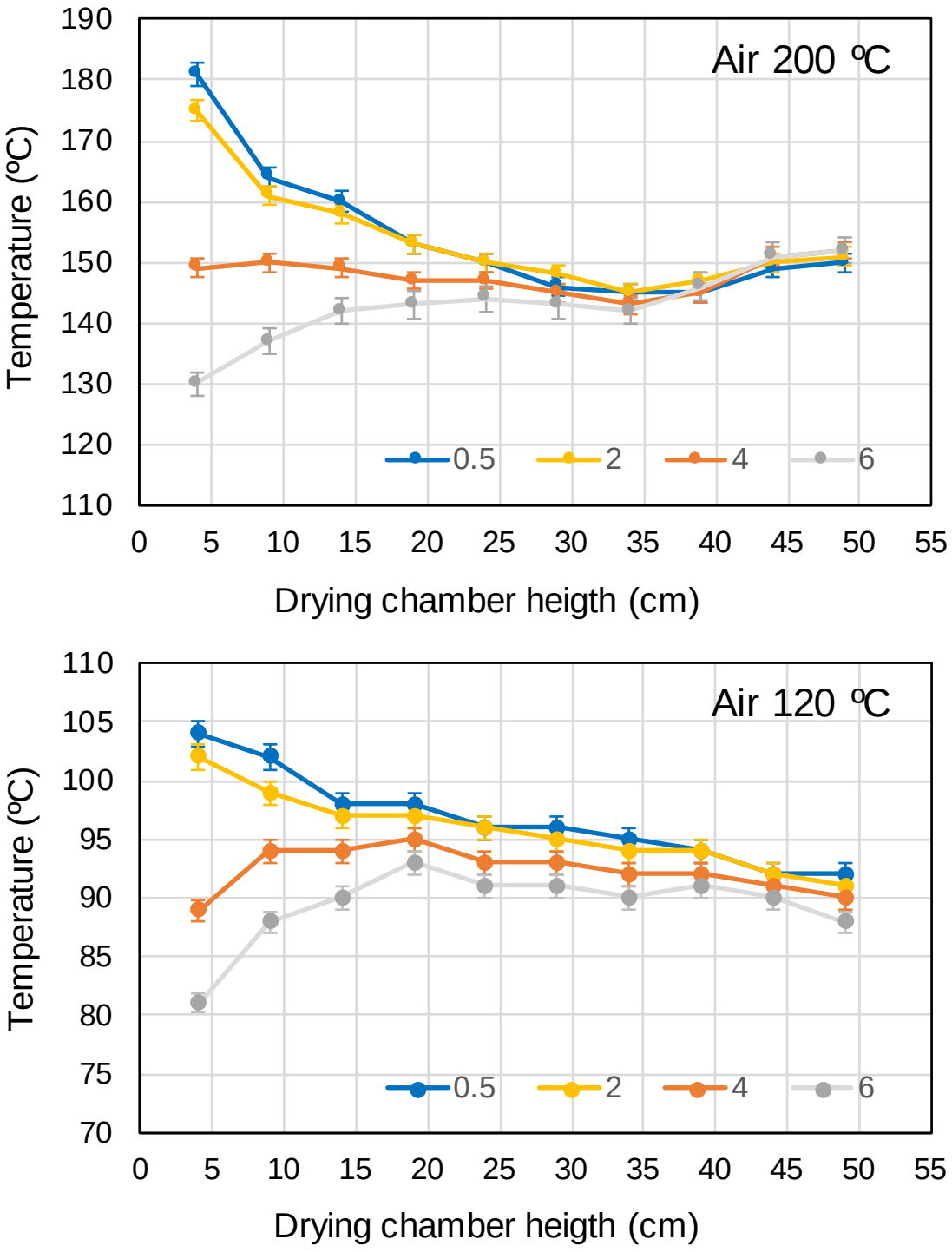

Figure 4

Figure 5

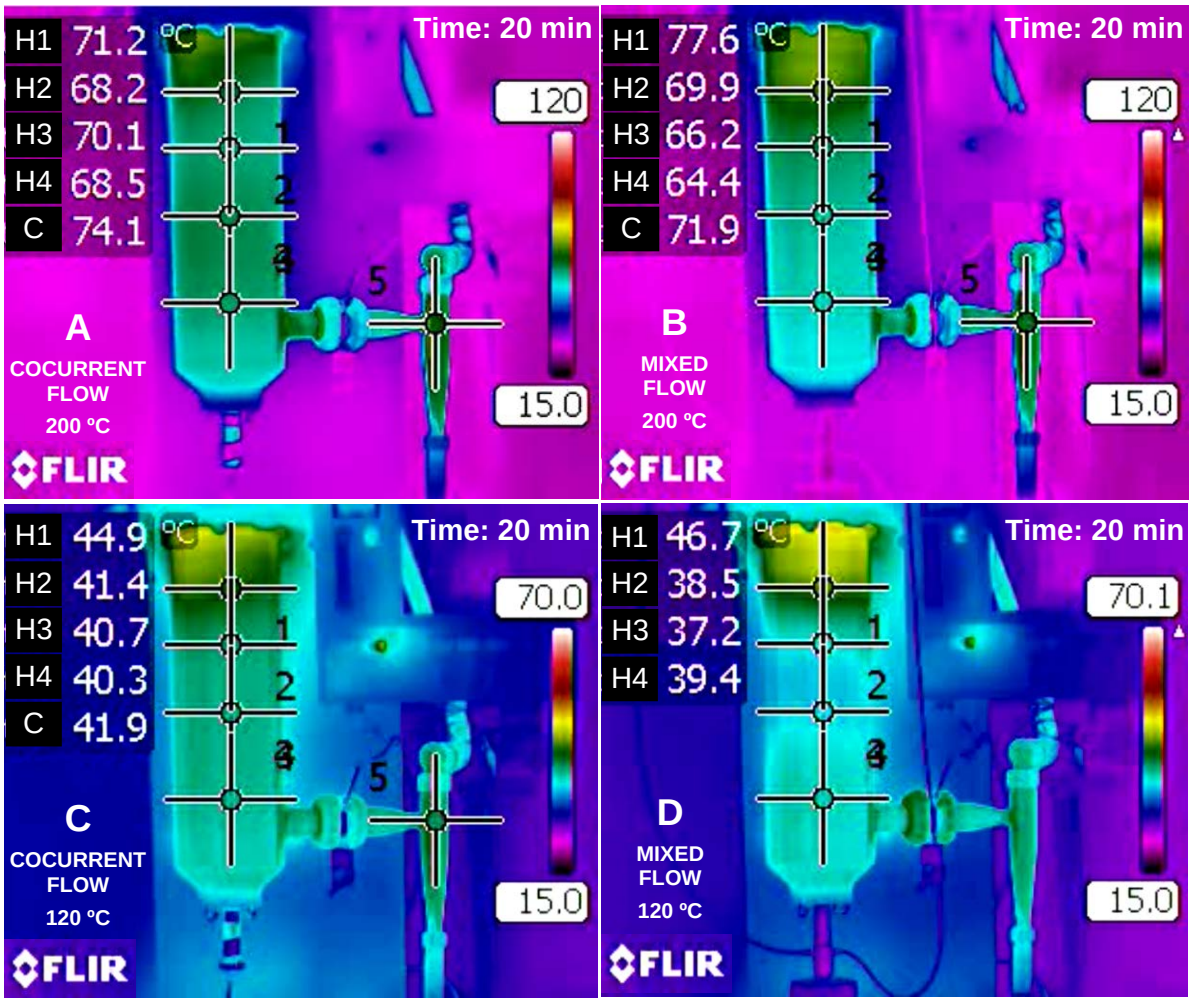

Figure 5

New Figure 6

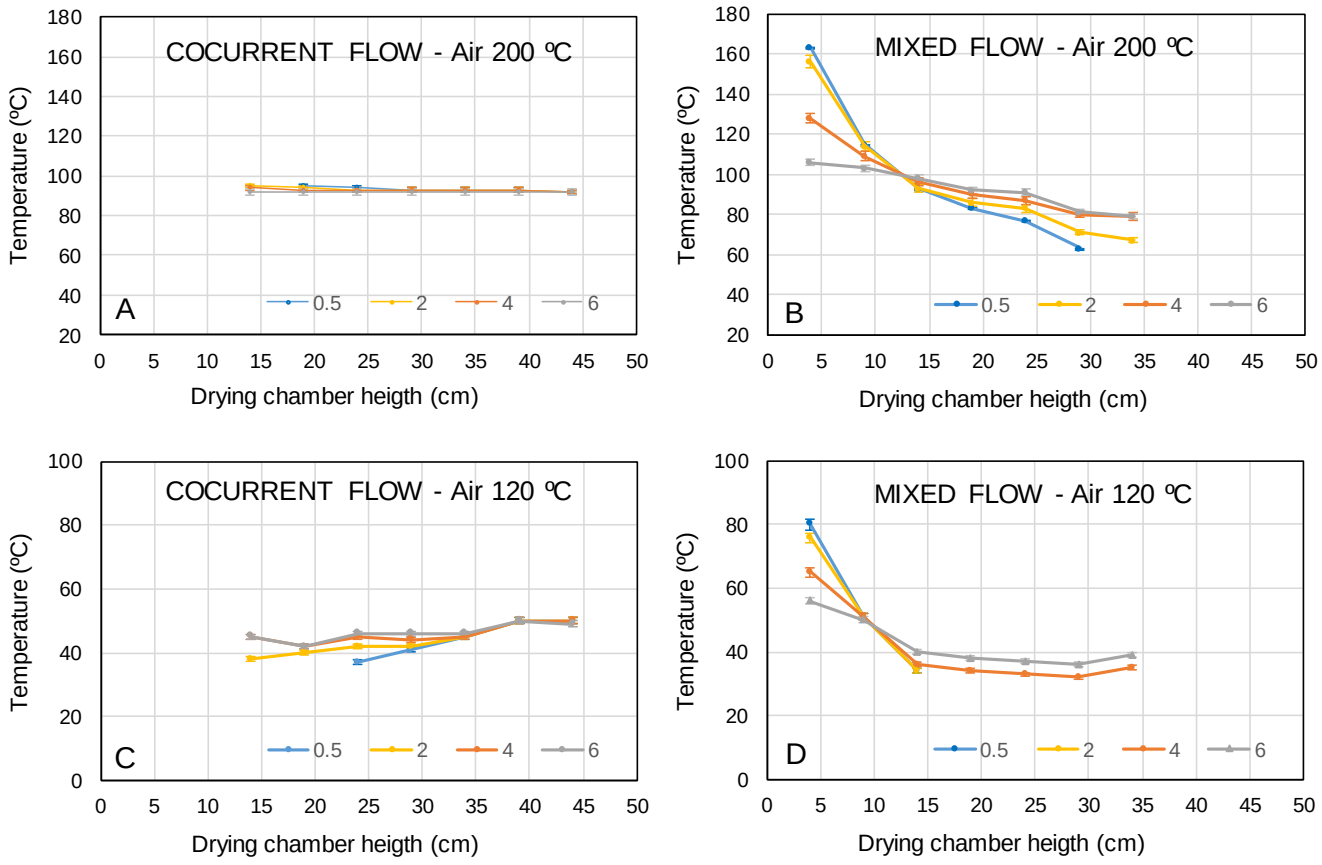

Figure 6

Figure 7

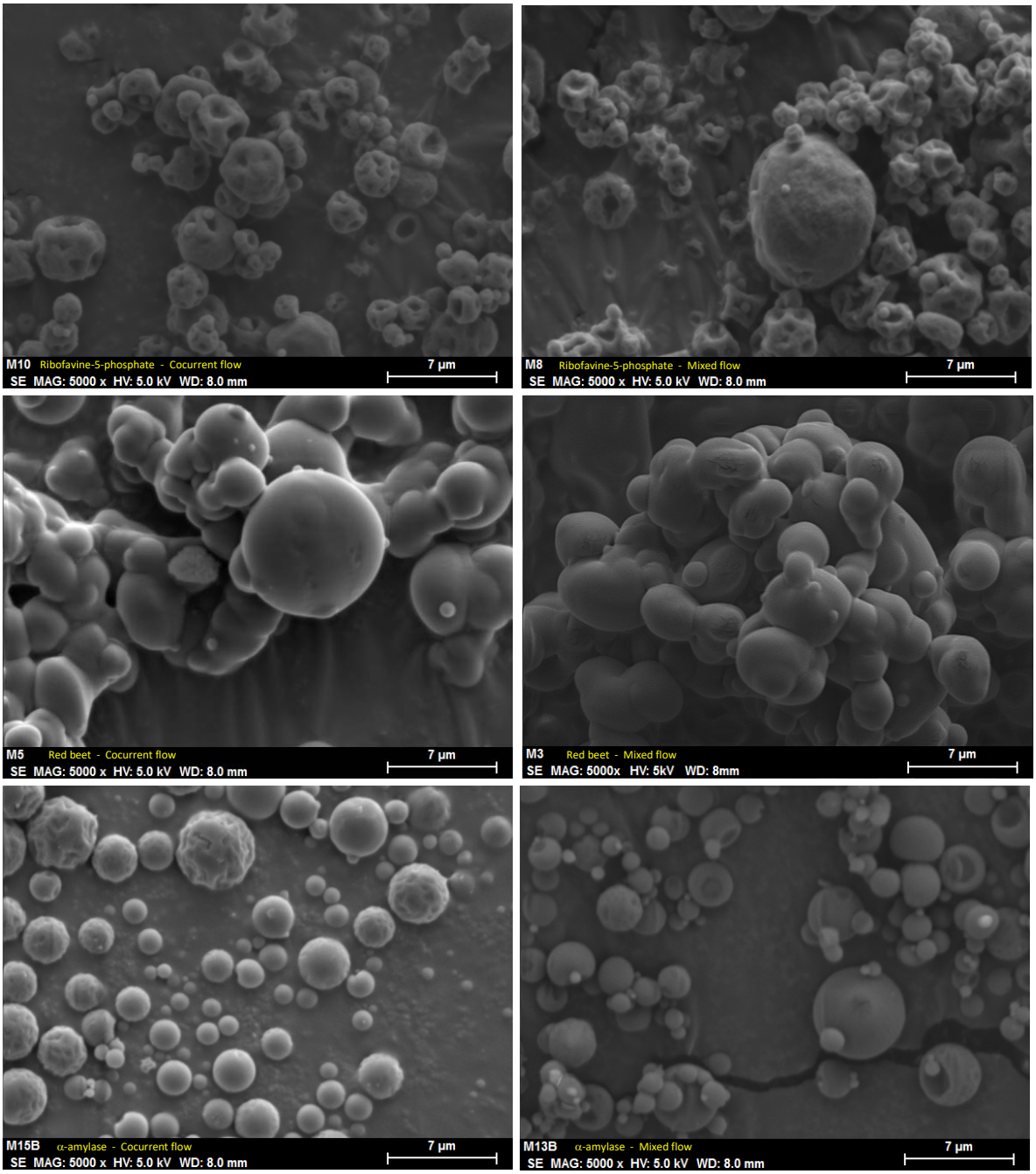

Figure 7

Figure Legends

Figure 1. Schematic drawing of the lab-scale spray drying equipment. A. Drying chamber working with cocurrent or mixed flow, B. Inlet of drying air located in the upper part of the chamber, C. Up-view of equipment showing inlet of drying air (+) and locations of temperature thermocouples (●).

Figure 2. Thermographic images at different times of the spray drying equipment during operation with inlet air at 200 ºC (A: 5 min, B: 15 min, C: 30 min). Zoom images of upper zone of drying chamber at steady state conditions taken from different camera positions (D,E,F). Evolution of surface temperatures in positions H1-H4 with time (G).

Figure 3. Filled contour plot of temperatures inside drying chamber during operation with inlet air at 200 ºC.

Figure 4. Temperature profiles inside drying chamber at 0.5, 2, 4 and 6 cm of central axis during operation with inlet air at 200 ºC and 120 ºC.

Figure 5. Thermographic images at steady state conditions during spray drying of water at 200 and 120 ºC, with cocurrent (A, C) and mixed flow (B,D), respectively.

Figure 6. Temperature profiles inside drying chamber at 0.5, 2, 4 and 6 cm of central axis during spray drying of water at 200 and 120 ºC, with cocurrent (A, C) and mixed flow (B,D), respectively.

Figure 7. Morphology of bioactive compounds powders obtained by spray drying at 200 ºC with cocurrent (A, C, E) and mixed flow (B, D, F). Riboflavine-5-phosphate (A,B), red beet (C, D) and α-amylase (E, F).

Table

Table 1. Evaluation of bioactive compounds spray drying performance using cocurrent and mixed flow with drying air at 200 and 120 ºC

Parameter	Cocurrent flow		Mixed flow	
	200 ºC	120 ºC	200 ºC	120 ºC
Riboflavine-5-phosphate				
Drying yield (%)	75.5 ± 1.3^{c}	71.5 ± 1.2^{b}	72.0 ± 1.4^{b}	63.0 ± 1.8^{a}
Color yield (%)	99.8 ± 0.2^{a}	99.7 ± 0.3^{a}	99.6 ± 0.2^{a}	99.8 ± 0.2^{a}
Outlet temperature (ºC)	86 ± 1^{c}	43 ± 1^{b}	84 ± 1^{c}	36 ± 1^{a}
Bulk density (Kg/m^3)	482 ± 7^{b}	348 ± 5^{a}	532 ± 3^{c}	490 ± 8^{b}
Water content (%)	2.1 ± 0.2^{b}	2.9 ± 0.4^{c}	1.6 ± 0.3^{a}	1.9 ± 0.3^{b}
Dissolution test (s)	95 ± 1^{b}	85 ± 2^{a}	105 ± 1^{d}	100 ± 3^{c}
Red beet				
Drying yield (%)	74.5 ± 1.5^{d}	68.5 ± 1.6^{c}	60.0 ± 1.2^{b}	52.5 ± 1.7^{a}
Color yield (%)	99.6 ± 0.3^{a}	99.7 ± 0.2^{a}	99.8 ± 0.1^{a}	99.7 ± 0.3^{a}
Outlet temperature (ºC)	89 ± 1^{c}	49 ± 1^{b}	87 ± 1^{c}	41 ± 1^{a}
Bulk density (Kg/m^3)	558 ± 8^{b}	532 ± 5^{a}	552 ± 7^{b}	537 ± 9^{a}
Water content (%)	2.5 ± 0.3^{b}	2.8 ± 0.3^{b}	1.6 ± 0.3^{a}	2.7 ± 0.3^{b}
Dissolution test (s)	150 ± 3^{c}	75 ± 4^{a}	140 ± 1^{b}	70 ± 5^{a}
α-amylase				
Drying yield (%)	66 ± 0.9^{c}	58 ± 1.3^{b}	65 ± 1.1^{c}	32 ± 1.4^{a}
Activity retention (%)	90.0 ± 0.6^{b}	99.2 ± 0.2^{c}	82.9 ± 0.4^{a}	91.1 ± 0.3^{b}
Outlet temperature (ºC)	87 ± 1^{c}	56 ± 0^{b}	85 ± 1^{c}	43 ± 0^{a}
Bulk density (Kg/m^3)	533 ± 3^{c}	475 ± 7^{a}	544 ± 9^{c}	510 ± 3^{b}
Water content (%)	1.4 ± 0.3^{a}	2.5 ± 0.3^{b}	0.9 ± 0.3^{a}	2.4 ± 0.3^{b}
Dissolution test (s)	50 ± 1^{b}	40 ± 2^{a}	48 ± 1^{b}	35 ± 3^{a}

Means having different letters indicate significant differences within each raw at $p \leq 0.05$ (Tukey's test).